Research Paper

Development of Rutin–Quercetin Loaded Nanostructured Lipid Carrier Dispersions for Acne: Fractional Factorial Design Optimisation and Characterisation

Bhati Jaya[1], Parvez Nayyar[1*], Jain Neha[2] and Singh Amarjeet[3]

[1]School of Pharmacy, Sharda University, Greater Noida, Uttar Pradesh, India
[2]Centre for Pharmaceutics, Amity Institute of Pharmacy, Amity University, Noida, Uttar Pradesh, India
[3]Innovative College of Pharmacy, Greater Noida, Uttar Pradesh, India
Corresponding Author: Parvez Nayyar, *nparvez2013@gmail.com*

Abstract

Nanostructured lipid carriers (NLCs) promote drug penetration and retention within the skin and are therefore attractive vehicles for the topical management of acne vulgaris. The present work formulated and optimised a rutin–quercetin co-loaded NLC dispersion using a design-of-experiments approach. A 2^3 fractional factorial design examined the influence of the solid-to-liquid lipid ratio (X_1), the surfactant-to-co-surfactant ratio (X_2) and sonication time (X_3) on particle size, polydispersity index (PDI) and entrapment efficiency. Stearic acid and eucalyptus oil constituted the lipid matrix, stabilised by poloxamer 188 and Tween 80. The eight design runs yielded dispersions of 175 ± 10 to 286 ± 23 nm with PDI values of 0.274 to 0.485 and entrapment efficiencies of 94.45 ± 3.4 to 98.64 ± 4.0%. All regression models were statistically significant ($p < 0.05$), with coefficients of determination of 0.9229, 0.9835 and 0.9390 for particle size, PDI and entrapment efficiency respectively. Desirability-based optimisation identified formulation FF1 (lipid ratio 65:35, surfactant ratio 1:1, sonication 6 min), which exhibited a particle size of 228 ± 29 nm, PDI of 0.24, zeta potential of −16.3 ± 0.9 mV and entrapment efficiency of 98.05 ± 4.3%. Transmission electron microscopy confirmed discrete spherical vesicles, in vitro release followed the Korsmeyer–Peppas model ($R^2 = 0.994$, $n = 0.49$) indicating non-Fickian diffusion and the dispersion remained stable for 60 days under refrigerated and ambient storage.

Keywords: Nanostructured lipid carrier, Topical delivery, Design of experiments, Acne vulgaris, Flavonoids, Rutin, Quercetin.

Introduction

Acne vulgaris is a chronic inflammatory disorder of the pilosebaceous unit and one of the most prevalent dermatological conditions worldwide. Although it is not life-threatening, it exerts a considerable influence on confidence, self-esteem and quality of life and frequently demands prolonged and persistent therapy[32,41]. The condition presents with inflammatory and non-inflammatory lesions comprising open and closed comedones, papules, pustules, nodules and cysts, which may resolve with scarring and post-inflammatory pigmentation[41].

The pathogenesis of acne is multifactorial. Elevated sebum secretion by the sebaceous glands, follicular hyperkeratinisation, the release of lipids and free fatty acids into the follicular lumen and the resulting inflammation together create an anaerobic microenvironment favourable to *Cutibacterium* (*Propionibacterium*) *acnes*. Prolonged exposure to conventional antibiotics has driven resistance in these organisms, partly through modification of the bacterial cell wall, so that the competition between antibiotic and microorganism is persistent and topical antibacterial therapy has become progressively less reliable[42].

Plant-derived actives have consequently attracted renewed interest. Bacteria are less likely to develop resistance against phytoconstituents because such molecules act on multiple targets simultaneously, and several flavonoids display activity against *P. acnes* and *Staphylococcus epidermidis*-induced acne vulgaris[30,39]. Rutin (quercetin-3-*O*-rutinoside) is a bioflavonoid with documented antioxidant, anti-inflammatory and antiproliferative activity that also modulates intracellular signalling cascades[27]. Quercetin, its aglycone, is among the most widely studied dietary flavonoids and displays anti-inflammatory, antiviral and antitumour potential[4,35]; its cutaneous delivery has been examined in oleogels, nanosponges and mesoporous carriers[10,35,39]. Eucalyptus oil, obtained from the leaves of *Eucalyptus* species, contributes antimicrobial and anti-inflammatory activity while acting as a permeation promoter. Both flavonoids are, however, poorly water soluble and unstable at the skin surface, which restricts their direct topical use.

Nanostructured lipid carriers (NLCs) are second-generation lipid nanoparticles composed of a blend of solid and liquid lipids[25,36]. The liquid lipid disrupts the crystalline order of the solid matrix and creates imperfections that accommodate drug molecules, so that NLCs overcome the limited loading capacity and drug expulsion associated with solid lipid nanoparticles and offer good stability, high loading and controlled release[34,36]. On dermal application they adhere to the stratum corneum, form an occlusive film, hydrate the skin and enhance the cutaneous bioavailability of the incorporated actives[16,24,28]. These attributes have established NLCs as a widely adopted platform for topical therapy[3,9,40], and carriers have been reported for anti-acne agents including adapalene[26], dapsone[1], spironolactone[6] and clarithromycin[37] as well as for conventional anti-acne

combinations[20,21], natural actives such as thymol[18,44], propolis[19] and violacein[11] and a range of other topical indications[7,13,17].

Fractional factorial designs permit several formulation factors to be screened simultaneously with a small number of experimental runs, reduce cost and reliably identify the dominant factors and interactions that govern product quality[15,46]. The present work therefore formulates a rutin–quercetin co-loaded NLC dispersion intended for acne and applies a 2^3 fractional factorial design to optimise lipid ratio, surfactant ratio and sonication time against particle size, polydispersity index and entrapment efficiency.

Material and Methods

Materials: Rutin was procured from CDH Pvt. Ltd. and quercetin from Yucca Enterprises Ltd. Eucalyptus oil was obtained from Moksha Pvt. Ltd. Stearic acid and methyl para-benzoate were purchased from CDH Chemicals, New Delhi, India. Poloxamer 188 and Tween 80 were of pharmaceutical grade. All other reagents and chemicals used in the study were of laboratory grade.

Calibration curves: Stock solutions were prepared by dissolving 10 mg each of rutin and quercetin in 10 mL of ethanol in separate volumetric flasks. Serial dilutions covering 0–12 µg/mL were prepared in phosphate-buffered saline (PBS) pH 7.4 and the absorbance was recorded on a UV–visible spectrophotometer (Lab India Analytical UV3200) at 264 nm and 371 nm respectively[5,23].

Determination of the isosbestic point: The isosbestic point, that is the wavelength of equal absorptivity of the two flavonoids, was located by recording overlain spectra of mixtures of rutin and quercetin at varying composition in PBS pH 7.4 against a solvent blank over the ultraviolet range. Quercetin exhibited λ_{max} at 371 nm and rutin at 264 nm; the common intersection of the spectra of the mixed solutions was taken as the isosbestic wavelength[5].

Drug–excipient compatibility: Fourier-transform infrared (FT-IR) spectra (Perkin Elmer) were acquired for rutin, quercetin, the excipients and their 1:1 physical mixture after storage in separate glass vials at room temperature for 15 days, using the KBr pellet method. Spectra were scanned over 4000–400 cm^{-1} and the observed bands were assigned and compared against reference spectra[27].

Selection of the solid lipid: Molten stearic acid was combined with the liquid lipid in ratios of 1:9, 2:8, 3:7, 4:6, 5:5, 6:4, 7:3, 8:2 and 9:1 and the blends were stirred magnetically at 200 rpm and 75 ± 2 °C for 1 h. After cooling, each blend was applied to Whatman No. 1 filter paper and examined under ultraviolet and visible light. Any oil droplet remaining on the paper indicated immiscibility of the binary blend; visual inspection was performed in parallel[12,43].

Selection of the liquid lipid: The solubility of rutin and quercetin was determined in cinnamon, turpentine, peppermint, clove, orange and eucalyptus oils. An excess of each flavonoid was added to 2 mL of oil in Eppendorf tubes and shaken to equilibrium at ambient temperature for 48 h. Samples were centrifuged, the supernatant was withdrawn, the flavonoids were extracted into ethanol and the ethanolic solutions were assayed at 264 nm and 371 nm[12].

Screening of surfactant and co-surfactant: The oil-solubilising capacity of Tween 80, poloxamer 188, PEG 400 and Tween 20 was determined by titration. A 15% v/v aqueous surfactant solution was prepared in double-distilled water and 1.5 mL was titrated with 5 µL aliquots of the selected oil under vigorous shaking until turbidity appeared, the end point denoting maximum oil-solubilising capacity. The influence of surfactant concentration (0.5, 1.5 and 2.5% w/v) on entrapment efficiency was subsequently evaluated[12,14,29].

Experimental design: A three-factor, two-level fractional factorial design (FFD) was employed. The independent variables were the solid-to-liquid lipid ratio (X_1), the surfactant-to-co-surfactant ratio (X_2) and the sonication time (X_3); the dependent responses were particle size (Y_1), polydispersity index (Y_2) and entrapment efficiency (Y_3). The design generated eight runs. The levels, goals and importance assigned to each variable are given in Table 1[15,46].

Table 1: Independent variables, levels, dependent responses and constraints applied in the 2^3 fractional factorial design

Variable	Low level (−1)	High level (+1)	Goal	Importance
X_1 = solid lipid : liquid lipid ratio	60:40	70:30	Within range	+ + +
X_2 = surfactant : co-surfactant ratio	1:1	2:1	Within range	+ + +
X_3 = sonication time (min)	4	6	Within range	+ + +
Y_1 = particle size (nm)	—	—	Minimise	+ + +

Variable	Low level (−1)	High level (+1)	Goal	Importance
Y_2 = polydispersity index	—	—	Minimise	+ + +
Y_3 = entrapment efficiency (%)	—	—	Maximise	+ + +

Preparation of NLC dispersions: Rutin and quercetin (1:1) were accurately weighed and dispersed in the molten solid–liquid lipid blend of stearic acid and eucalyptus oil in the proportions specified by the design, and the mixture was melted at 70 °C to give a homogeneous lipid phase. The aqueous phase, comprising 2.5% w/v poloxamer 188 with Tween 80 as co-surfactant in double-distilled water, was heated separately to 70 °C for 10 min. The aqueous phase was added slowly to the lipid phase and the amalgamation was stirred at 600 rpm and 75 °C for 1 h to yield the primary emulsion, which was then probe-sonicated in a single cycle for the time specified by the design. The emulsion was rapidly cooled in an ice bath to give the NLC dispersion, which was centrifuged at 12,000 rpm for 10 min to remove insoluble raw material and oversized particles[30,36,39].

Optimisation by the desirability function: The approach of Derringer and Suich was used to optimise the three responses simultaneously. Each variable and response was assigned a goal, and an individual desirability ranging from 0 (undesirable) to 1 (most desirable) was computed and combined into an overall desirability so that the optimum could be located within the design space[8].

Particle size, polydispersity index and zeta potential: Mean particle size and PDI of the quercetin-loaded (QNLC), rutin-loaded (RNLC) and combined (RQNLC) dispersions were measured by dynamic light scattering using photon correlation spectroscopy (Malvern Zetasizer Nano ZS 90). Samples were diluted appropriately with double-distilled water to avoid multiple scattering and analysed at 25 ± 1 °C at a fixed scattering angle of 90°, after equilibration to eliminate air bubbles. The Z-average hydrodynamic diameter was recorded as particle size. Zeta potential was determined by electrophoretic light scattering (Zetasizer ZEN3600, Malvern Analytical Ltd., UK) on samples diluted with double-distilled water. All measurements were performed in triplicate and are reported as mean ± standard deviation[33].

Entrapment efficiency: Ten millilitres of the dispersion were transferred to a glass tube, sonicated in a bath sonicator for 10 min and centrifuged at 9000 rpm and 20 °C for 30 min. The supernatant was assayed by UV spectroscopy at the isosbestic wavelength of 384 nm and the entrapment efficiency was calculated as equation (1)[33].

$$EE\ (\%) = [(\text{Total drug} - \text{Free drug}) / \text{Total drug}] \times 100 \quad (1)$$

In vitro drug release: Release was studied in a Franz diffusion cell (borosilicate glass, 25 mL receptor capacity, 2.0 cm diffusion diameter) using the dialysis membrane technique. A dialysis membrane of 12–14 kDa molecular weight cut-off was cut to size and soaked in PBS pH 7.4 for 48 h before use. The receptor compartment was filled with PBS pH 7.4 and the pre-treated membrane was mounted at the open end. Aliquots were withdrawn at predetermined intervals with replacement by fresh medium and assayed spectrophotometrically. The release data of the three dispersions were fitted to zero-order, first-order, Higuchi, Korsmeyer–Peppas and Hixson–Crowell models and the regression coefficient of each model was compared[4,38].

Stability studies: The optimised RQNLC dispersion was stored for 60 days under refrigeration (4 °C), at ambient temperature (25 °C) and under accelerated conditions of 40 ± 2 °C and 75 ± 5% relative humidity in accordance with ICH guidelines, and particle size, PDI, zeta potential and entrapment efficiency were monitored[22,45].

Transmission electron microscopy: The morphology of the optimised dispersion was examined with a transmission electron microscope (JEOL JEM-F200). The dispersion was diluted with pre-filtered distilled water, negatively stained with 1% phosphotungstic acid, mounted on a copper grid, dried and imaged at an accelerating voltage of 100 kV[31].

Results and Discussion

Preformulation studies: Rutin showed an absorption maximum at 264 nm and quercetin at 371 nm in ethanol with subsequent dilution in PBS pH 7.4. Linear calibration curves were obtained over 0–12 µg/mL and are presented in Figure 1. The regression equations were Y = 0.060x + 0.001 for rutin and Y = 0.046x + 0.009 for quercetin, with coefficients of determination of 0.9971 and 0.9895 respectively, confirming adherence to the Beer–Lambert law and the accuracy of the dilution series[5,23].

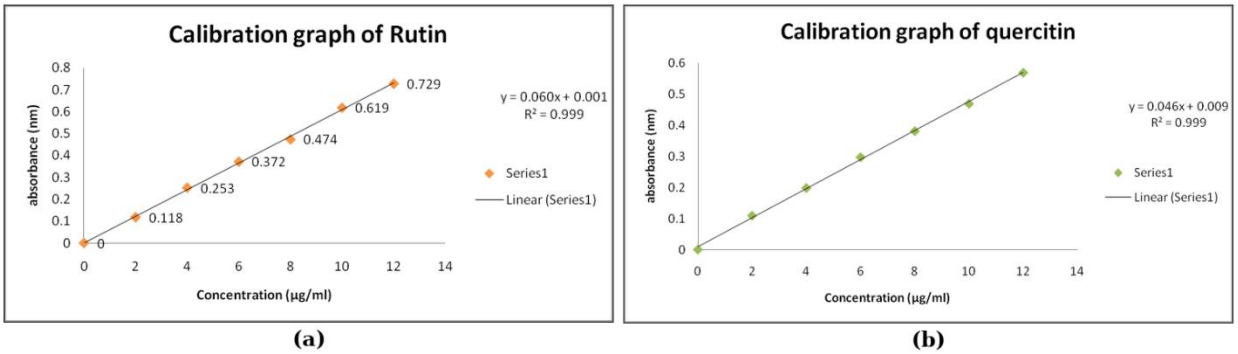


Figure 1: Calibration curves of (a) rutin at 264 nm and (b) quercetin at 371 nm in phosphate-buffered saline pH 7.4

The overlain spectra of the mixed solutions intersected at 384 nm, at which both flavonoids exhibit identical absorptivity (Figure 2). This wavelength is therefore suitable for the simultaneous estimation of the two actives without mutual interference and was adopted for all entrapment-efficiency measurements[5,23].

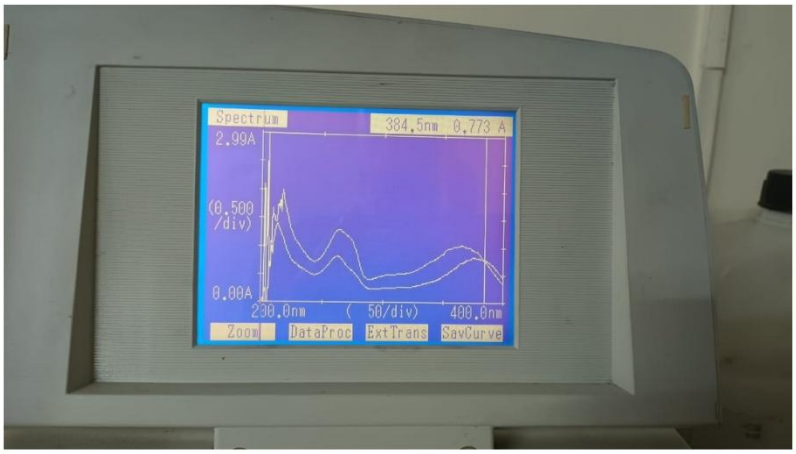


Figure 2: Overlain ultraviolet spectra of rutin and quercetin mixtures showing the isosbestic point at 384 nm

The FT-IR spectra of pure rutin, pure quercetin, the 1:1 rutin–quercetin combination and the physical mixture with stearic acid recorded after 15 days of storage are shown in Figure 3, and the assigned bands are compiled in Tables 2 to 5. The characteristic phenolic O–H stretching band near 3200–3600 cm^{-1}, the flavonoid carbonyl band at approximately 1660–1650 cm^{-1} and the aromatic C=C stretching bands at 1600–1500 cm^{-1} were retained in the physical mixture without displacement, and no additional band appeared. The absence of new peaks confirms that no chemical interaction occurred between the flavonoids and the excipients and that the selected excipients are suitable for formulation development[27].

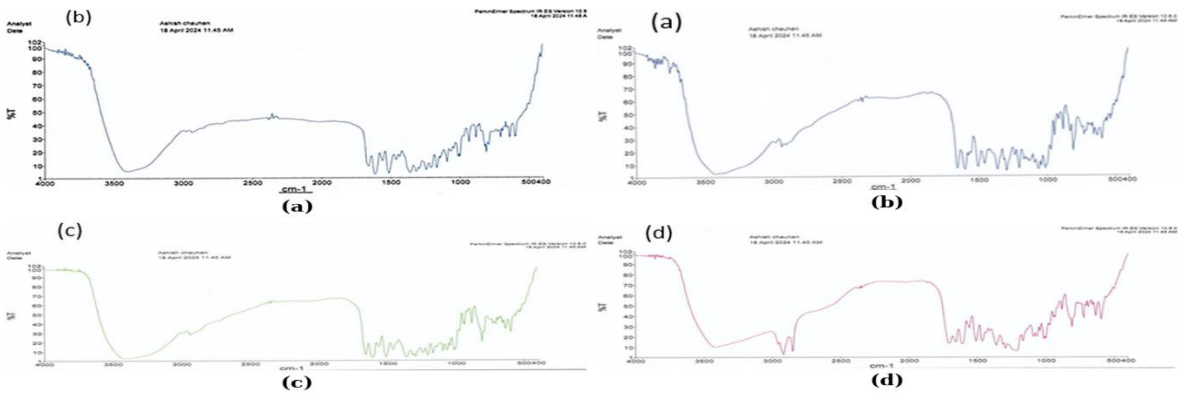


Figure 3: FT-IR spectra of (a) rutin, (b) quercetin, (c) the rutin–quercetin combination and (d) the physical mixture with excipients

Table 2: Observed FT-IR wavenumbers and assigned functional groups of rutin

S. No.	Functional group / assignment	Wavenumber (cm^{-1})
1	C–O stretching (alcohol / ether)	1400–1000
2	Carboxylic O–H	3400–3200
3	Alkane C–H	3000–2850
4	Aromatic C–H	3150–3050
5	Aromatic ring	1600
6	C=C	1495
7	Alkane C–H bending	1550
8	C=O	1700
9	Aromatic out-of-plane bending	900–600

Table 3: Observed FT-IR wavenumbers and assigned functional groups of quercetin

S. No.	Functional group / assignment	Wavenumber (cm^{-1})
1	O–H, free and hydrogen-bonded phenols	3650–3600
2	Amine C–N	1350–1000
3	Alcohol / carboxylic acid C–O	1300–1000
4	Aromatic ring	1600
5	C–O stretching	1200
6	Out-of-plane bending	600, 678, 800, 920
7	O–H stretching	3400
8	C–CO–C	1150
9	Aromatic C=C ring stretching	1615–1510

Table 4: Observed FT-IR wavenumbers and assigned functional groups of the rutin–quercetin combination

S. No.	Functional group / assignment	Wavenumber (cm^{-1})
1	O–H stretching, broad, phenolic (strong hydrogen bonding)	3600–3200
2	C–H stretching (aromatic / aliphatic)	3000–2850
3	C=O stretching, flavonoid ketone	1660–1650
4	Aromatic C=C stretching	1600–1500
5	C–C / C–H bending	1450–1400
6	C–O stretching	1300–1000
7	C–O stretching	1200–1150
8	C–O of secondary alcohol (sugar moiety of rutin)	1100–1000
9	=C–H bending, aromatic	900–700
10	Skeletal vibrations	700–500

Table 5: Observed FT-IR wavenumbers and assigned functional groups of the physical mixture

S. No.	Functional group / assignment	Wavenumber (cm^{-1})
1	O–H stretching	3500–3200
2	Aliphatic C–H stretching from lipid / surfactant excipients	2950–2850
3	C=O stretching, ester	1730–1700
4	C=O stretching, flavonoid	1660–1630
5	Aromatic C=C stretching	1600–1500

S. No.	Functional group / assignment	Wavenumber (cm^{-1})
6	C–H bending	1450–1370
7	C–O stretching, phenolic and ether groups	1300–1150
8	C–O–C stretching	1150–1000
9	C–O / C–C vibrations	1000–800
10	Aromatic C–H bending	800–600

Selection of lipids and surfactants: Stearic acid and eucalyptus oil formed a homogeneous binary blend that left no residual oil droplet on the filter paper and produced the highest entrapment of the two flavonoids, and were therefore selected as the solid and liquid lipid respectively. The lipid phase provides a matrix that accommodates the active moiety and retains it until release[12,43]. Among the surfactants screened, poloxamer 188 with Tween 80 as co-surfactant gave the greatest oil-solubilising capacity. Entrapment efficiency rose with surfactant concentration and 2.5% w/v was sufficient to encapsulate the maximum quantity of drug, values of 96–98% being obtained; concentrations beyond this gave no further improvement, which is consistent with saturation of the particle surface and the onset of micelle formation[14,29].

Fractional factorial design: Eight runs were prepared and analysed for particle size (Y_1), polydispersity index (Y_2) and entrapment efficiency (Y_3). The design matrix with observed and predicted responses is given in Table 6 and the model statistics in Table 7. Predicted-versus-actual plots for the three responses are shown in Figure 4 and the corresponding three-dimensional response surfaces in Figure 5.

Table 6: Design matrix with observed and predicted responses of the eight design runs and the optimised formulation

Run	X_1	X_2	X_3 (min)	Particle size (nm)		Entrapment efficiency (%)		Polydispersity index	
				Observed	Predicted	Observed	Predicted	Observed	Predicted
F1	60:40	2:1	6	237 ± 11	175	98.64 ± 4.0	97.42	0.287	0.471
F2	60:40	1:1	6	184 ± 11	221	97.31 ± 3.9	97.42	0.448	0.411
F3	70:30	2:1	4	175 ± 10	184	97.42 ± 3.8	98.31	0.471	0.348
F4	60:40	1:1	4	221 ± 20	245	97.42 ± 3.4	95.90	0.411	0.275
F5	70:30	2:1	6	286 ± 23	196	98.22 ± 4.2	98.64	0.274	0.436
F6	70:30	1:1	6	245 ± 29	237	96.90 ± 3.0	94.45	0.275	0.287
F7	70:30	1:1	4	247 ± 14	247	96.21 ± 4.2	96.21	0.485	0.485
F8	60:40	2:1	4	196 ± 9	186	94.45 ± 3.4	98.22	0.436	0.274
FF1	**65:35**	**1:1**	**6**	**228 ± 29**	**231**	**98.05 ± 4.3**	**97.34**	**0.24**	**0.26**

FF1 denotes the optimised formulation obtained by the desirability-function approach.

Effect of the independent variables on particle size: The coded polynomial relating the significant terms to Y_1 is given as equation (2).

$$Y_1 = 211.38 + (-26.13)\, X_2 + (4.63)\, X_1X_2 \quad (2)$$

The sign and magnitude of each coefficient indicate the direction and extent of the corresponding effect; positive coefficients denote a synergistic contribution and negative coefficients an antagonistic one. The negative coefficient of X_2 shows an inverse relationship between surfactant ratio and particle size, an increase in surfactant reducing interfacial tension and stabilising the nascent nanoparticles against coalescence. Sonication supplies the energy needed to disintegrate larger droplets into the nanometric range, while the positive X_1X_2 interaction indicates that a balance between lipid and surfactant is required to reach the desired dimensions. The model was significant ($F = 29.91$, $p = 0.0017$) with $R^2 = 0.9229$ and a coefficient of variation of 4.59%[14,29].

Effect of the independent variables on polydispersity index: The coded polynomial for Y_2 is given as equation (3).

$$Y_2 = 0.3734 + (-0.0156)\, X_1 + (0.0279)\, X_3 + (-0.0554)\, X_1X_3 + (0.0434)\, X_2X_3 + (0.0281)\, X_1X_2X_3 \quad (3)$$

PDI values ranged from 0.274 to 0.485 across the design. Values below 0.3 denote a homogeneous and stable nanoparticle population whereas higher values indicate heterogeneity, and the lowest PDI of 0.274 was recorded for run F5. Sonication time exerted a positive main effect but interacted negatively with the lipid ratio

(X_1X_3), showing that particle homogeneity depends on an appropriate combination of lipid content and sonication energy. The positive X_2X_3 interaction indicates that excessive sonication in the presence of a high surfactant concentration can promote instability and broaden the distribution. The difference between adjusted and predicted R^2 was within the accepted limit of 0.2 and the model was significant (F = 23.87, p = 0.0407).

Effect of the independent variables on entrapment efficiency: The coded polynomial for Y_3 is given as equation (4).

$$Y_3 = 97.07 + (1.08)\ X_2 + (0.4963)\ X_1X_2 + (0.5512)\ X_1X_2X_3 \quad (4)$$

Entrapment efficiency ranged from 94.45 ± 3.4 to 98.64 ± 4.0% across the design, confirming efficient incorporation of both flavonoids within the lipid matrix. All coefficients were positive, the surfactant ratio X_2 exerting the dominant beneficial effect: a higher surfactant concentration improves solubilisation of the flavonoids in the lipid melt and stabilises the interface, so that a greater proportion of drug is retained within the particles. The model was significant (F = 20.82, p = 0.0067) with R^2 = 0.9835 and a coefficient of variation of 0.489%[29].

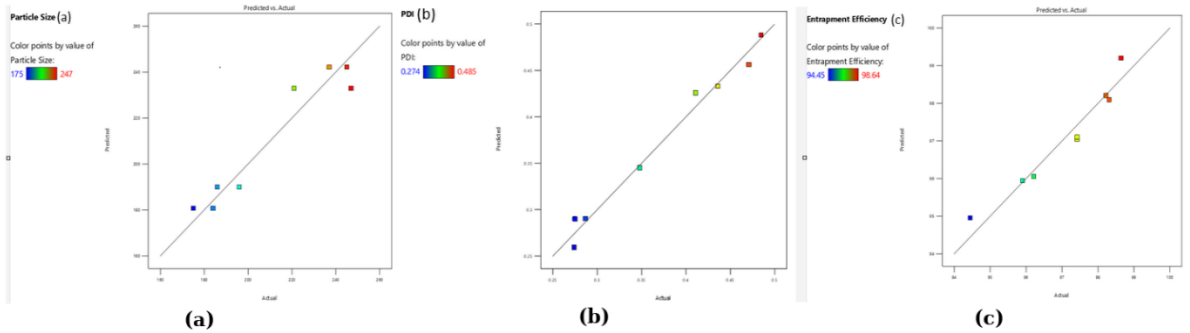


Figure 4: Predicted versus actual plots for (a) particle size, (b) polydispersity index and (c) entrapment efficiency

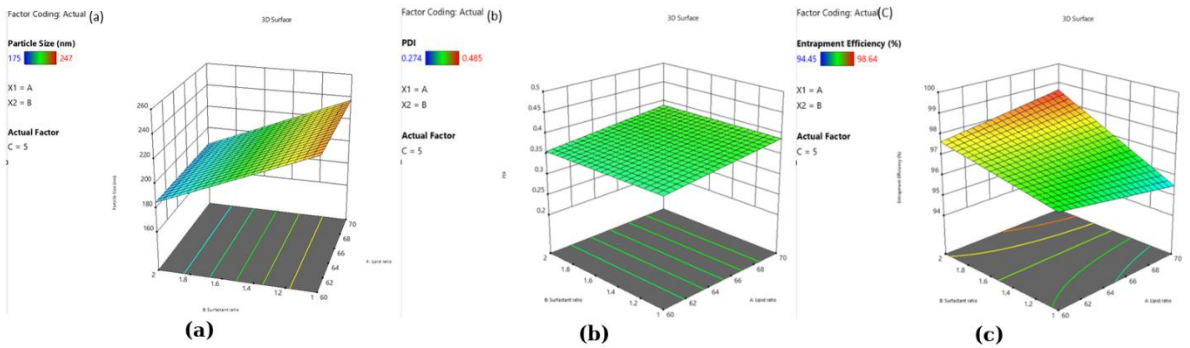


Figure 5: Three-dimensional response surfaces showing the effect of (a) lipid and surfactant ratio on particle size, (b) lipid ratio and sonication time on polydispersity index and (c) surfactant ratio and sonication time on entrapment efficiency

Table 7: Model fitting statistics and analysis of variance for the three responses

Response	Model	R^2	Adjusted R^2	Predicted R^2	SD	F value	p value	% CV
Particle size	Multiple regression	0.9229	0.8920	0.8026	9.70	29.91	0.0017	4.59
Polydispersity index	Multiple regression	0.9835	0.9423	0.7363	0.0213	23.87	0.0407	5.70
Entrapment efficiency	Multiple regression	0.9390	0.8947	0.7593	0.467	20.82	0.0067	0.489

Characterisation of the optimised dispersions: Application of the desirability function within the design space identified formulation FF1, prepared at a lipid ratio of 65:35, a surfactant ratio of 1:1 and 6 min of sonication. The observed responses of FF1 agreed closely with the predicted values (Table 6), which validates the models. The particle size, PDI and zeta potential of the individual and combined dispersions are given in Table 8, and the corresponding size distributions and zeta-potential traces are presented in Figures 6 and 7. All three dispersions carried a negative surface charge arising from the ionised carboxyl groups of stearic acid and the phenolic

hydroxyls of the flavonoids. The magnitude of the charge, together with the steric barrier contributed by poloxamer 188, accounts for the physical stability of the colloidal system[33].

Table 8: Particle size, polydispersity index and zeta potential of the optimised dispersions

Formulation code	Particle size (nm)	Polydispersity index	Zeta potential (mV)
QNLC (quercetin-loaded)	274.9 ± 11	0.20	−22.9 ± 1.1
RNLC (rutin-loaded)	271.2 ± 8	0.19	−19.4 ± 0.7
RQNLC (combination, FF1)	228.2 ± 13	0.24	−16.3 ± 0.9

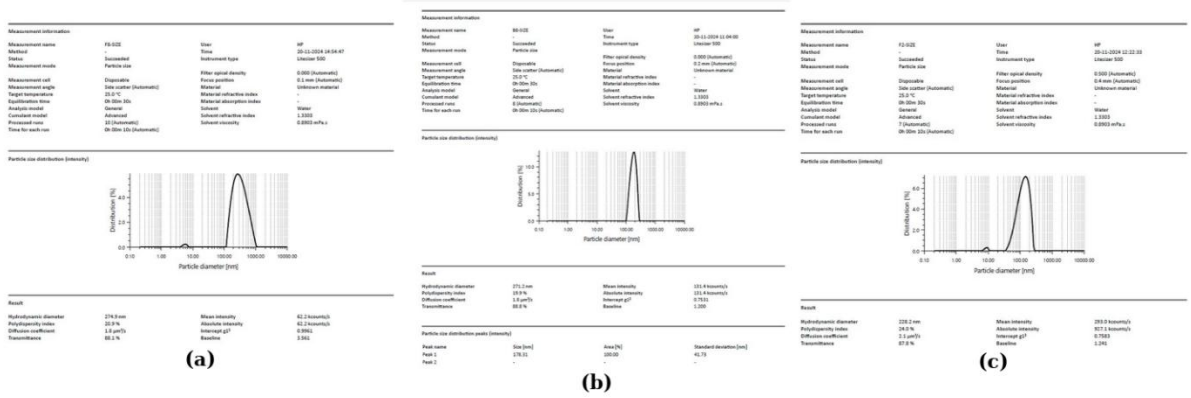


Figure 6: Particle size distributions of the optimised (a) QNLC, (b) RNLC and (c) RQNLC dispersions

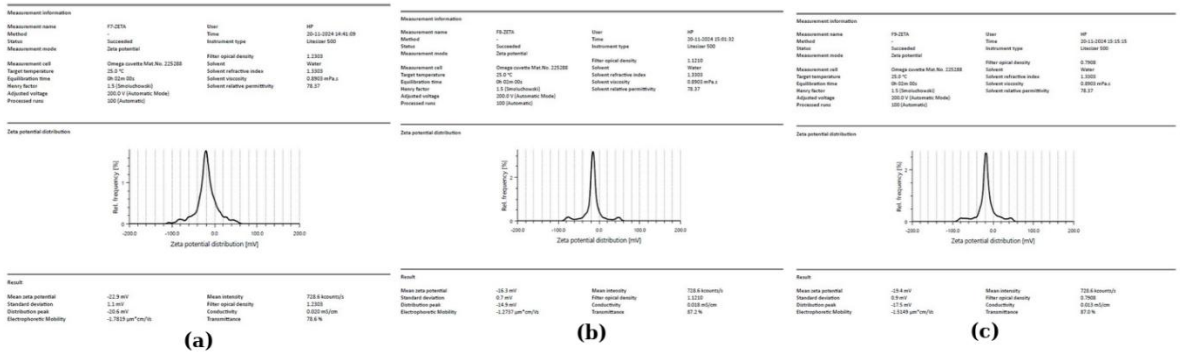


Figure 7: Zeta potential distributions of the optimised (a) QNLC, (b) RNLC and (c) RQNLC dispersions

The particle sizes obtained here lie within the range considered favourable for dermal application. Particles of roughly 200–400 nm adhere well to the stratum corneum and form an occlusive film that promotes hydration and penetration into the viable epidermis without appreciable systemic absorption[16,24,28]. Comparable dimensions have been reported for adapalene-, dapsone-, spironolactone- and clarithromycin-loaded carriers intended for acne[1,6,26,37] and for anti-acne combinations formulated as lipid nanoparticles[20,21], while carriers of natural actives such as thymol, propolis and violacein have been described in a similar size domain[11,18,19,44]. The entrapment efficiencies achieved in the present work are at the upper end of those reported for lipid-nanoparticle gels developed for other topical indications[2,7,13,17].

In vitro drug release and release kinetics: The release profiles of the QNLC, RNLC and RQNLC dispersions are shown in Figure 8. All three exhibited an initial rapid phase attributable to drug adsorbed at or near the particle surface, followed by a sustained phase governed by diffusion through the lipid matrix. The combined RQNLC dispersion released the flavonoids more gradually than either single-drug carrier, which is consistent with its smaller particle size and denser matrix. Comparable sustained profiles have been reported for quercetin delivered from oleogels, nanosponges and mesoporous silica carriers and for microemulsion-based topical systems[10,35,38,39].

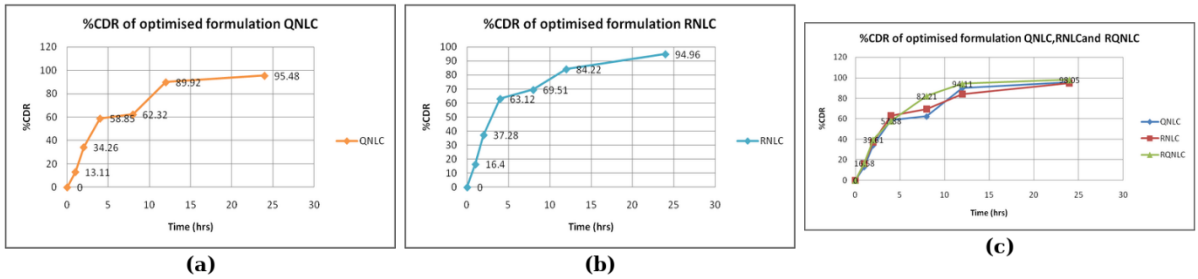


Figure 8: Cumulative percentage drug release from the (a) QNLC, (b) RNLC and (c) comparative profiles of the RQNLC, RNLC and QNLC dispersions

The release data were fitted to five kinetic models and the regression coefficients are compiled in Table 9, with the corresponding plots for the optimised dispersion shown in Figure 9. The RQNLC dispersion conformed best to the Korsmeyer–Peppas model (R^2 = 0.994) with a release exponent of 0.49, indicating anomalous or non-Fickian transport in which both diffusion through the lipid matrix and relaxation of the matrix itself govern release[4].

Table 9: Regression coefficients of the release kinetic models fitted to the three dispersions

S. No.	Formulation code	Zero order (R^2)	First order (R^2)	Higuchi (R^2)	Korsmeyer–Peppas (R^2)	Hixson–Crowell (R^2)
1	QNLC	0.778	0.935	0.950	0.971	0.896
2	RNLC	0.962	0.983	0.957	0.986	0.929
3	RQNLC	0.685	0.950	0.913	0.994	0.867

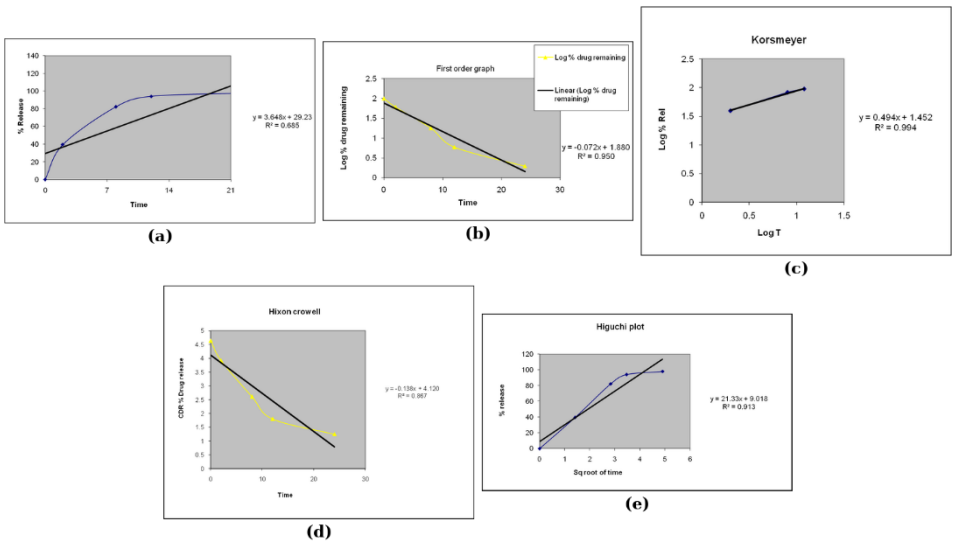


Figure 9: Release kinetic models fitted to the optimised RQNLC dispersion: (a) zero order, (b) first order, (c) Korsmeyer–Peppas, (d) Hixson–Crowell and (e) Higuchi

Morphology: The transmission electron micrograph of the optimised RQNLC dispersion (Figure 10) shows discrete, approximately spherical vesicles of uniform morphology without aggregation, confirming the successful formation of nanostructured lipid carriers. The dimensions observed by microscopy are consistent with the hydrodynamic diameters measured by dynamic light scattering, the small difference being attributable to the hydration layer contributing to the latter[28,31].

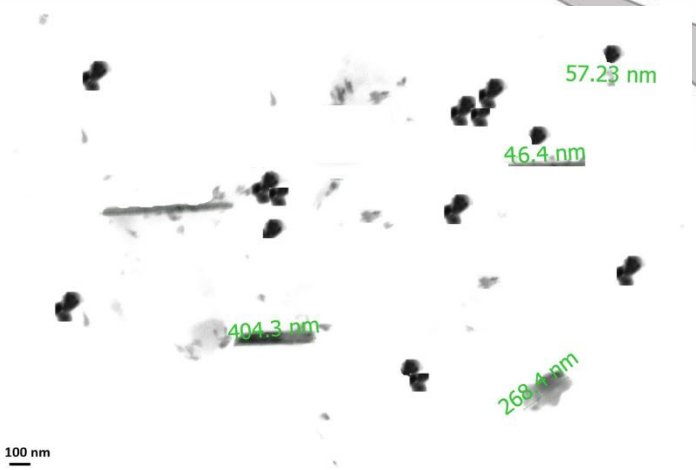


Figure 10: Transmission electron micrograph of the optimised RQNLC dispersion

Stability studies: Over 60 days the optimised dispersion remained essentially unchanged under refrigeration and at ambient temperature, showing only a marginal increase in particle size and PDI. Under accelerated conditions of 40 ± 2 °C and 75 ± 5% relative humidity a perceptible increase in particle size and slight aggregation were observed, accompanied by a small reduction in zeta potential and entrapment efficiency. The behaviour is consistent with partial recrystallisation of the lipid matrix and gradual loss of interfacial stabilisation at elevated temperature[16,22,45]. The dispersion therefore possesses good physical stability, particularly at lower storage temperatures, and incorporation into a semi-solid gel base is indicated for further improvement of stability and for convenient topical application.

Conclusion

Rutin–quercetin co-loaded nanostructured lipid carrier dispersions were successfully prepared by melt emulsification followed by probe sonication and were optimised using a 2^3 fractional factorial design. The design established that formulation variables exert a considerable and quantifiable influence on the physicochemical attributes of the dispersion. The lipid ratio affected particle size, higher lipid content tending to increase size through the greater viscosity of the lipid matrix, whereas the surfactant ratio lowered interfacial tension, improved the homogeneity of the dispersion and prevented particle aggregation. No further reduction in size was obtained beyond an optimal surfactant concentration, indicating saturation of the particle surface and probable micelle formation. The optimised formulation FF1 exhibited a particle size of 228 ± 29 nm, a polydispersity index of 0.24, a zeta potential of −16.3 ± 0.9 mV and an entrapment efficiency of 98.05 ± 4.3%, released the flavonoids by non-Fickian diffusion according to the Korsmeyer–Peppas model and remained stable for 60 days at refrigerated and ambient conditions. The dispersion therefore possesses adequate drug-carrying capacity, controlled release behaviour and colloidal stability, and represents a promising lipid-based platform for the topical delivery of flavonoids in acne[3,9]. Incorporation of the optimised dispersion into a gel base and evaluation of its ex vivo permeation and antimicrobial performance are proposed as the next stage of this work.

Conflict of Interest

The authors declare that there is no conflict of interest.

Data Availability

All data generated or analysed during this study are included in this published article.

Statement of Ethical Approval

Only in vitro studies were involved in this research work; no human or animal subjects were used.

Acknowledgement

The authors sincerely acknowledge the support and facilities provided by the School of Pharmacy, Sharda University, Greater Noida and express their gratitude to all contributors who assisted in this research work.

References

1. Ahmed T.A., Ibrahim H.M., Samy A.M. and Kaseem A.A., Dapsone-loaded nanostructured lipid carriers for topical delivery in acne treatment, *Int. J. Pharm.*, **567**, 118465 (**2019**)

2. Aiyalu R., Govindarjan A. and Ramasamy A., Formulation and evaluation of topical herbal gel for the treatment of arthritis in an animal model, *Braz. J. Pharm. Sci.*, **52**(3), 493-507 (**2016**)

3. Beloqui A., Solinís M.A., Rodríguez-Gascón A., Almeida A.J. and Préat V., Nanostructured lipid carriers: promising drug delivery systems for topical application, *J. Control. Release*, **238**, 63-77 (**2016**)
4. Casagrande R., Georgetti S.R., Verri W.A. Jr., Borin M.F., Lopez R.F. and Fonseca M.J., In vitro evaluation of quercetin cutaneous absorption from topical formulations and its functional stability by antioxidant activity, *Int. J. Pharm.*, **328**(2), 183-190 (**2007**)
5. Chaudhari S.P., Bangar J.V., Akuskar G.K. and Ratnaparkhi M.P., Development and validation of a UV spectrophotometric method for simultaneous estimation of rutin and quercetin in niosome formulation, *Der Pharm. Lett.*, **6**(3), 271-276 (**2014**)
6. Chen H., Chang X., Du D., Li J., Xu H. and Yang X., Spironolactone-loaded nanostructured lipid carriers for topical acne treatment, *J. Dermatolog. Treat.*, **27**(6), 567-574 (**2016**)
7. Chhowala I.S., Patel S. and Shah P., Development of a nanoparticulate drug delivery system for acne treatment, *Int. J. Pharm. Res. Technol.*, **13**(1), 45-52 (**2023**)
8. Costa N.R., Lourenço J. and Pereira Z.L., Desirability function approach: a review and performance evaluation in adverse conditions, *Chemom. Intell. Lab. Syst.*, **107**(2), 234-244 (**2011**)
9. Doktorovova S., Souto E.B. and Silva A.M., Nanostructured lipid carriers for topical drug delivery, *Eur. J. Pharm. Biopharm.*, **88**(1), 1-12 (**2014**)
10. Elmowafy M., Musa A., Alnusaire T.S., Shalaby K., Fouda M.M., Salama A., Al-Sanea M.M., Abdelgawad M.A., Gamal M. and Fouad S.A., Olive oil/pluronic oleogels for skin delivery of quercetin: in vitro characterization and ex vivo skin permeability, *Polymers*, **13**(11), 1808 (**2021**)
11. Ferreira M., Rocha S. and Ribeiro A., Violacein extract loaded nanostructured lipid carriers for dermal anti-acne formulations, *Key Eng. Mater.*, **901**, 129-135 (**2021**)
12. Gaba B., Fazil M., Khan S., Ali A., Baboota S. and Ali J., Nanostructured lipid carrier system for topical delivery of terbinafine hydrochloride, *Bull. Fac. Pharm. Cairo Univ.*, **53**(2), 147-159 (**2015**)
13. Garg N.K., Tyagi R.K., Singh B. and Sharma G., Nanostructured lipid carrier-mediated transdermal delivery of aceclofenac hydrogel, *Front. Pharmacol.*, **13**, 821266 (**2022**)
14. Han F., Li S., Yin R., Liu H. and Xu L., Effect of surfactants on the formation and characterization of a new type of colloidal drug delivery system: nanostructured lipid carriers, *Colloids Surf. A Physicochem. Eng. Asp.*, **315**(1-3), 210-216 (**2008**)
15. Jaynes J., Ding X., Xu H., Wong W.K. and Ho C.M., Application of fractional factorial designs to study drug combinations, *Stat. Med.*, **32**(2), 307-318 (**2013**)
16. Jenning V., Gysler A., Schäfer-Korting M. and Gohla S.H., Vitamin A loaded solid lipid nanoparticles for topical use: occlusive properties and drug targeting to the upper skin, *Eur. J. Pharm. Biopharm.*, **49**(3), 211-218 (**2000**)
17. Kharwade R.S., Mahajan N.M. and More H.N., Formulation and evaluation of a nanostructured lipid carrier based anti-inflammatory gel, *Asian J. Pharm. Clin. Res.*, **12**(5), 210-215 (**2019**)
18. Khezri K., Saeedi M. and Maleki Dizaj S., Gel-dispersed nanostructured lipid carriers loaded with thymol for dermal applications, *Pharmaceutics*, **16**(1), 95 (**2024**)
19. Khodadadi M., Jafari S.M. and Assadpour E., Propolis-loaded nanostructured lipid carriers: formulation and antimicrobial activity, *BMC Complement. Med. Ther.*, **22**, 312 (**2022**)
20. Kumari S., Pandita D. and Poonia N., Nanostructured lipid carriers for topical delivery of anti-acne drugs: formulation and characterization, *Pharm. Nanotechnol.*, **3**(3), 174-184 (**2015**)
21. Lala R. and Nandvikar N., Development and evaluation of nanostructured lipid carriers for acne therapy, *J. Pharm. Res. Int.*, **33**(40), 121-129 (**2021**)
22. Lohan S. and Bhatia M., Amphotericin B-loaded nanostructured lipid carrier gel: preparation and evaluation for enhanced skin permeation, *Biomed. Pharmacol. J.*, **18**(2) (**2025**)
23. Majithia R.H., Khodadiya A. and Patel V.B., Spectrophotometric method development and validation for simultaneous estimation of anagliptin and metformin HCl by the Q-absorption ratio method in a synthetic mixture, *Heliyon*, **6**(5), e03855 (**2020**)
24. Müller R.H., Petersen R.D., Hommoss A. and Pardeike J., Nanostructured lipid carriers (NLC) in cosmetic dermal products, *Adv. Drug Deliv. Rev.*, **59**(6), 522-530 (**2007**)
25. Müller R.H., Radtke M. and Wissing S.A., Nanostructured lipid matrices for improved microencapsulation of drugs, *Int. J. Pharm.*, **242**(1-2), 121-128 (**2002**)
26. Nasrollahi S.A., Taghibiglou C. and Azizi E., Preparation and evaluation of adapalene nanostructured lipid carriers for targeted drug delivery in acne, *Dermatol. Ther.*, **34**(1), e14777 (**2021**)
27. Paczkowska M., Lewandowska K., Bednarski W., Mizera M., Podborska A., Krause A. and Cielecka-Piontek J., Application of spectroscopic methods for identification (FT-IR, Raman spectroscopy) and determination (UV, EPR) of quercetin-3-O-rutinoside: experimental and DFT based approach, *Spectrochim. Acta A Mol. Biomol. Spectrosc.*, **140**, 132-139 (**2015**)
28. Pardeike J., Hommoss A. and Müller R.H., Lipid nanoparticles (SLN, NLC) in cosmetic and pharmaceutical dermal products, *Int. J. Pharm.*, **366**(1-2), 170-184 (**2009**)

29. Pezeshki A., Ghanbarzadeh B., Mohammadi M., Fathollahi I. and Hamishehkar H., Encapsulation of vitamin A palmitate in nanostructured lipid carrier (NLC): effect of surfactant concentration on the formulation properties, *Adv. Pharm. Bull.*, **4**(Suppl. 2), 563-568 (**2014**)
30. Pivetta T.P., Silva L.B., Kawakami C.M., Araújo M.M., Del Lama M.P. and Naal R.M., Topical formulation of quercetin encapsulated in natural lipid nanocarriers: evaluation of biological properties and phototoxic effect, *J. Drug Deliv. Sci. Technol.*, **53**, 101148 (**2019**)
31. Puglia C., Sarpietro M.G., Bonina F., Castelli F., Zammataro M. and Chiechio S., Development, characterization and in vitro and in vivo evaluation of benzocaine- and lidocaine-loaded nanostructured lipid carriers, *J. Pharm. Sci.*, **100**(5), 1892-1899 (**2011**)
32. Qureshi M., Qadir A., Aqil M., Sultana Y., Warsi M.H., Ismail M.V. and Talegaonkar S., Berberine loaded dermal quality by design adapted chemically engineered lipid nano-constructs-gel formulation for the treatment of skin acne, *J. Drug Deliv. Sci. Technol.*, **66**, 102805 (**2021**)
33. Rajinikanth P.S. and Chellian J., Development and evaluation of nanostructured lipid carrier-based hydrogel for topical delivery of 5-fluorouracil, *Int. J. Nanomedicine*, **11**, 5067-5077 (**2016**)
34. Rizwanullah M., Amin S. and Ahmad J., Improved pharmacokinetics and antihyperlipidemic efficacy of rosuvastatin-loaded nanostructured lipid carriers, *J. Drug Target.*, **25**(1), 58-74 (**2017**)
35. Sapino S., Ugazio E., Gastaldi L., Miletto I., Berlier G., Zonari D. and Oliaro-Bosso S., Mesoporous silica as topical nanocarriers for quercetin: characterization and in vitro studies, *Eur. J. Pharm. Biopharm.*, **89**, 116-125 (**2015**)
36. Shah R., Eldridge D., Palombo E. and Harding I., Nanostructured lipid carriers: a novel drug delivery system, *Curr. Drug Deliv.*, **12**(2), 163-171 (**2015**)
37. Shettigar P. and Koland M., Formulation and evaluation of clarithromycin loaded nanostructured lipid carriers for acne treatment, *J. Pharm. Res. Int.*, **33**(35), 150-158 (**2021**)
38. Soliman S.M., Malak N.A., El-Gazayerly O.N. and Rehim A.A., Formulation of microemulsion gel systems for transdermal delivery of celecoxib: in vitro permeation, anti-inflammatory activity and skin irritation tests, *Drug Discov. Ther.*, **4**(6), 459-471 (**2010**)
39. Sujitha Y.S. and Muzib Y.I., Formulation and optimization of quercetin loaded nanosponges topical gel: ex vivo, pharmacodynamic and pharmacokinetic studies, *Int. J. Appl. Pharm.*, **11**(5), 156-165 (**2019**)
40. Supriya N., Priya P., Ankita W. and Kayande K., Nanostructured lipid carriers: a promising approach for topical drug delivery system, *Int. J. Pharm. Sci. Med.*, **6**(7), 81-101 (**2021**)
41. Tuchayi S.M., Makrantonaki E., Ganceviciene R., Dessinioti C., Feldman S.R. and Zouboulis C.C., Acne vulgaris, *Nat. Rev. Dis. Primers*, **1**(1), 15029 (**2015**)
42. Vasam M., Korutla S. and Bohara R.A., Acne vulgaris: a review of the pathophysiology, treatment and recent nanotechnology based advances, *Biochem. Biophys. Rep.*, **36**, 101578 (**2023**)
43. Vieira R., Severino P., Nalone L.A., Souto S.B., Silva A.M., Lucarini M., Durazzo A., Santini A. and Souto E.B., Sucupira oil-loaded nanostructured lipid carriers (NLC): lipid screening, factorial design, release profile and cytotoxicity, *Molecules*, **25**(3), 685 (**2020**)
44. Vieira R., Severino P. and Souto E.B., Thymol-loaded nanostructured lipid carriers for dermal delivery, *Int. J. Pharm.*, **642**, 123150 (**2024**)
45. Yasir A.S., Suryaneta S., Handayani K.Y. and Satria B., Stability and irritation testing using the patch test method of a combination gel formulation containing aloe vera and basil leaf extracts, *Indones. J. Cosmet.*, **1**(1), 1-10 (**2023**)
46. Younes I., Ghorbel-Bellaaj O., Chaabouni M., Rinaudo M., Souard F., Vanhaverbeke C., Jellouli K. and Nasri M., Use of a fractional factorial design to study the effects of experimental factors on chitin deacetylation, *Int. J. Biol. Macromol.*, **70**, 385-390 (**2014**)